Journal Pre-proofs

Molecular Mechanisms by which Tetrahydrofuran Affects CO_2 Hydrate Growth: Implications for Carbon Storage

Anh Phan, Henrik Schlösser, Alberto Striolo

PII: S1385-8947(21)01011-1
DOI: https://doi.org/10.1016/j.cej.2021.129423
Reference: CEJ 129423

To appear in: *Chemical Engineering Journal*

Received Date: 19 December 2020
Revised Date: 11 March 2021
Accepted Date: 15 March 2021

Please cite this article as: A. Phan, H. Schlösser, A. Striolo, Molecular Mechanisms by which Tetrahydrofuran Affects CO_2 Hydrate Growth: Implications for Carbon Storage, *Chemical Engineering Journal* (2021), doi: https://doi.org/10.1016/j.cej.2021.129423

Molecular Mechanisms by which Tetrahydrofuran Affects CO_2 Hydrate Growth: Implications for Carbon Storage

Anh Phan, Henrik Schlösser,** and Alberto Striolo*

Department of Chemical Engineering, University College London, London, WC1E 7JE, UK

*Corresponding Author

a.striolo@ucl.ac.uk

** Current address:

Institute of Technical Thermodynamics, RWTH Aachen University, Aachen, 52062 Germany

Keywords: Molecular dynamics, CO_2 diffusion, hydrate thickness, CO_2 gas uptake

Abstract

Gas hydrates have attracted siginifcant fundamental and applied interests due to their important role in various technological and enviromental processes. More recently, gas hydrates have shown potential applications for greenhouse gas capture and storage. To facilitate the latter application, introducing chemical additives into clathrate hydrates could help to enhance hydrate formation/growth rates, provided the gas storage capacity is not reduced. Employing equilibrium molecular dynamics, we study the impact of tetrahydrofuran (THF) on the kinetics of carbon dioxide (CO_2) hydrate growth/dissociation and on the CO_2 storage capacity of hydrates. Our simulations reproduce experimental data for CO_2 and CO_2+THF hydrates at selected operating conditions. The simulated results confirm that THF in stoichiometric concentration does reduce CO_2 storage capacity. This is not only due to the shortage of CO_2 trapping in sII hydrate 5^{12} cages, but also because of the favored THF occupancy in hydrate cages due to preferential THF−water hydrogen bonds. An analysis of the dynamical properties for CO_2 and THF at the hydrate-liquid interface reveals that THF can expedite CO_2 diffusion yielding a shift in the conditions conducive to CO_2 hydrate growth and stability to lower pressures and higher temperatures compared to systems without THF. These simulation results augment literature experimental observations, as they provide needed insights into the molecular mechanisms that can be adjusted to achieve optimal CO_2 storage in hydrates.

Introduction

Clathrate hydrates are solid-like inclusion compounds formed under appropriate pressure and temperature conditions; in these structures, hydrogen-bonded water molecules assemble into crystalline polyhedron cages of variable sizes stabilized by guest molecules [1]. Gas hydrates have received great scientific and industrial attention [2-8] with the early stage of gas hydrate-related research focusing on flow assurance to prevent oil and gas pipeline blockage by hydrate formation. Currently, the growth of interest in the hydrate research field inclines towards the expansion of gas hydrate applications in water-energy-environment nexus including water desalination [9, 10], gas separations [11, 12], intermittent natural gas and hydrogen storage [13-17], refrigeration and transport [18, 19]. Further, attention is today focused on approaches to mitigate global warming through long-term CO_2 capture and sequestration, which could be achieved via the formation of CO_2 hydrates [20-24].

The utilization of CO_2 hydrates in Carbon Capture and Storage (CCS) applications [20] shows promise because of their environmentally friendly nature and cost-effectiveness compared to other CCS technologies such as chemical adsorption/absorption methods using adsorbate/amine [25-27], followed by CO_2 injection into geological formations [20, 28, 29]. For example, capturing one ton of CO_2 via the "Simteche Hydrate CO_2 Capture Process" costs $23.6 and $25.3 when hydrate-based and conventional absorption processes are implemented, respectively [30]. To render hydrate-based CO_2 capture technologies sustainable and economically viable, it is necessary to ensure that the hydrates show high stability and are generated at substantial growth rates. To achieve these goals, chemical additives could promote hydrate formation and growth. Such additives are categorized into thermodynamic and kinetic promoters [20, 31-33]. By engaging in hydrate formation, thermodynamic promoters can shift the stability conditions to lower pressures and higher temperatures compared to pristine systems without promoters. Kinetic promoters, on the other hand, are principally surfactants, which accelerate hydrate growth without participating in the hydrate structure itself [20]. THF is a well-known thermodynamic promoter employed as co-guests in sII hydrate structure together with other guests such as methane, hydrogen and CO_2 [14, 34-37]. Torre et al. studied experimentally the impact of both kinetic (SDS) and thermodynamic (THF) promoters on the CO_2

hydrate formation kinetics and showed that the rates are significantly enhanced when both additives are present in comparison to cases when only individual or no additives were used [31]. Veluswamy et al. [16, 32] investigated the influence of THF promoters on the kinetics of CH_4 and CO_2 hydrates formed under analogous driving force and temperature and pressure conditions; they observed differences in gas uptake and kinetics of CH_4 and CO_2 hydrates with correlated morphology changes caused by the guest. To maximise guest gas uptake, it would be desirable to only employ kinetic promoters, although thermodynamic promoters stabilise the systems and allow for milder conditions to be maintained during operations. Achieving fundamental insights into the molecular mechanisms by which different additives are efficient is required for identifying the optimal conditions, which could lead to improving gas storage capabilities and lowering operation costs as well as energy consumption.

Implementing atomistic molecular dynamics (MD) simulations, we investigate here the effect of THF, at various operating conditions, on CO_2 gas storage capacity and CO_2 hydrate growth/dissociation rates. We document CO_2 hydrate growth/dissociation rate, CO_2 gas uptake, differences in hydrate morphology with focus on the hydrate-liquid interface, and dynamical properties of CO_2 guest molecules. The simulation results validate the interpretation of experimental observations reported in the literature, and further highlight the mechanisms that could be triggered to optimise the technologies implemented for CO_2 capture and storage in hydrates. In the remainder of the manuscript, we first present the methodologies implemented for this investigation, we then discuss the results, and we conclude by summarising the key observations and their practical implications.

Simulation Methodology

Model Setup. Liquid-hydrate two-phase models were used for the simulations of CO_2 hydrate growth/dissociation. The sI hydrate structures were employed as the solid substrate for CO_2 gas hydrate. To build the initial configurations, we adopted a unit cell of sI CO_2 hydrate from the work of Takeuchi et al. [38]. The sI CO_2 hydrate unit cell was replicated four times in all directions ($4.812 \times 4.812 \times 4.812$ nm^3) to generate the hydrate slab. The hydrate slab was surrounded by water and CO_2 molecules, yielding a simulation box length of 16 nm in the *Z* direction. The hydrate substrate was then aligned to the *X*-*Y* plane. The *X* and *Y* dimensions of the simulation box are 4.812 and 4.812 nm, respectively. Applying periodic boundary conditions in all directions, the hydrate substrate model is effectively infinite along the *X* and *Y* directions.

Two systems are considered: CO_2 hydrates without and with THF, as illustrated in the left and right panels of **Figure 1**, respectively. The number of THF and CO_2 molecules inserted into the bulk aqueous liquid phase were 100 and 240, respectively, yielding the initial mole fractions of ~1.42% and ~3.27-3.45%, respectively. THF has a significant impact on the equilibrium temperature of CO_2-THF hydrates at concentrations < 2.75 mol % THF, while it only slightly affects the equilibrium conditions at 2.75 – 5.56 mol % [39, 40]. At high THF concentrations (> 5.56 mol %), THF inhibits the CO_2 hydrate formation [41]. At the conditions chosen here, THF is expected to stabilize the CO_2 hydrate.

Force Fields. Water molecules were simulated by the TIP4P/Ice model [42]. The TIP4P/Ice model has been proven successful to study hydrate nucleation and growth [43, 44] and to describe the properties of liquid state at ambient conditions [42]. CO_2 was modelled using the EPM2 force field [45], which is appropriate for quantifying the growth/dissociation mechanisms of CO_2 gas hydrates [46, 47]. THF was modelled employing the General AMBER Force Field (GAFF2) [48]. All nonbonded interactions were described by electrostatic and dispersion forces. The Coulombic potential was used to characterize the electrostatic interactions, with the particle–particle particle–mesh (PPPM) method for treating long-range corrections [49]. The 12−6 Lennard-Jones (LJ) potentials were used to model dispersive interactions. The Lorentz−Berthelot combining rules were employed to describe the LJ parameters for unlike interactions from the values of like components [50]. The cutoff distance of 14 Å was used for all interactions.

Implementation. Equilibrium MD simulations were carried out using the package GROMACS [51, 52]. We employed simulation procedures similar to those used in our previous study [7]. Initially, we performed an energy minimization protocol to relax high-energy initial configurations using the steepest descent method. The simulations were then conducted in the NVT canonical ensemble. These simulations were conducted for 250 ps to relax the initial configuration while the hydrate layer was kept fixed at the chosen temperatures. Subsequently, the simulations were performed within the isothermal-isobaric ensemble (NPT) under conditions appropriate for CO_2 hydrate growth/dissociation studies (T = 269.1-289.1 K and P = 25.5 bar). The temperatures were kept constant in the range from 269.1 to 289.1 K, inclusive, at 5 K interval, by a Nosé-Hoover thermostat [53, 54]. The approach implemented here is known as the 'direct coexistence method', which has been widely employed for studying crystal or hydrate growth/dissociation [47, 55-57]. The large size of our simulation system (~ 11044 molecules) helps reduce the impact of stochasticity in the determination of melting point; the uncertainty associated with melting point estimation with the direct coexistence method (smaller than 2 K) [47], allows us to satisfactorily employ 5 K interval in temperature to identify the molecular mechanisms responsible for hydrate growth/dissociation and to estimate the melting point of CO_2 gas hydrates. We set 0.5 ps as the time constant for coupling between the system and the thermostat, which guarantees to remove latent heat from the growing hydrate surface rather quickly [58]. The Parrinello−Rahman barostat was used to keep the pressure fixed at 25.5 bar [59], with the pressure coupling applied along the *Z* direction of the simulation box (perpendicular to the hydrate-liquid interface). Hence the simulation box lengths in the *X* and *Y* directions were maintained constant and the hydrate surface area was kept the same for all systems. The leapfrog algorithm with 1.0 fs time steps was used to integrate the equations of motion [60]. All molecules in the system, including water and CO_2 molecules within the hydrate surface, were allowed to move in the NPT simulations. We conducted each NPT simulation for at least 500 ns. The configurations of each system were extracted at different observation times *t*, e.g., 100, 200, 300, 400, and 500 ns; using these configurations as initial ones, all simulations were carried out for additional 2ns for data analysis. To quantify the uncertainty in our results, we performed two additional simulation runs for all systems with the same hydrate composition, albeit

different configurations for hydrate surfaces in contact with the liquid phase, at various temperatures. Sarupria et al. [61] and Míguez et al. [47] reported that using initial configurations of hydrate slabs with CO_2 occupancy values in the range from 100% to 87% shows no effect on melting point estimation for a hydrate-H_2O binary system. Míguez et al. [47] also reported that it is unlikely to estimate the hydrate-liquid CO_2 phase state equilibrium when the initial hydrate composition is of either 50% or 37.5%, because the hydrate slab dissociates. Therefore, we chose the initial CO_2 hydrate occupancy of 100% to identify the molecular growth/dissociation mechanisms of CO_2 gas hydrates, and how they change due to THF.

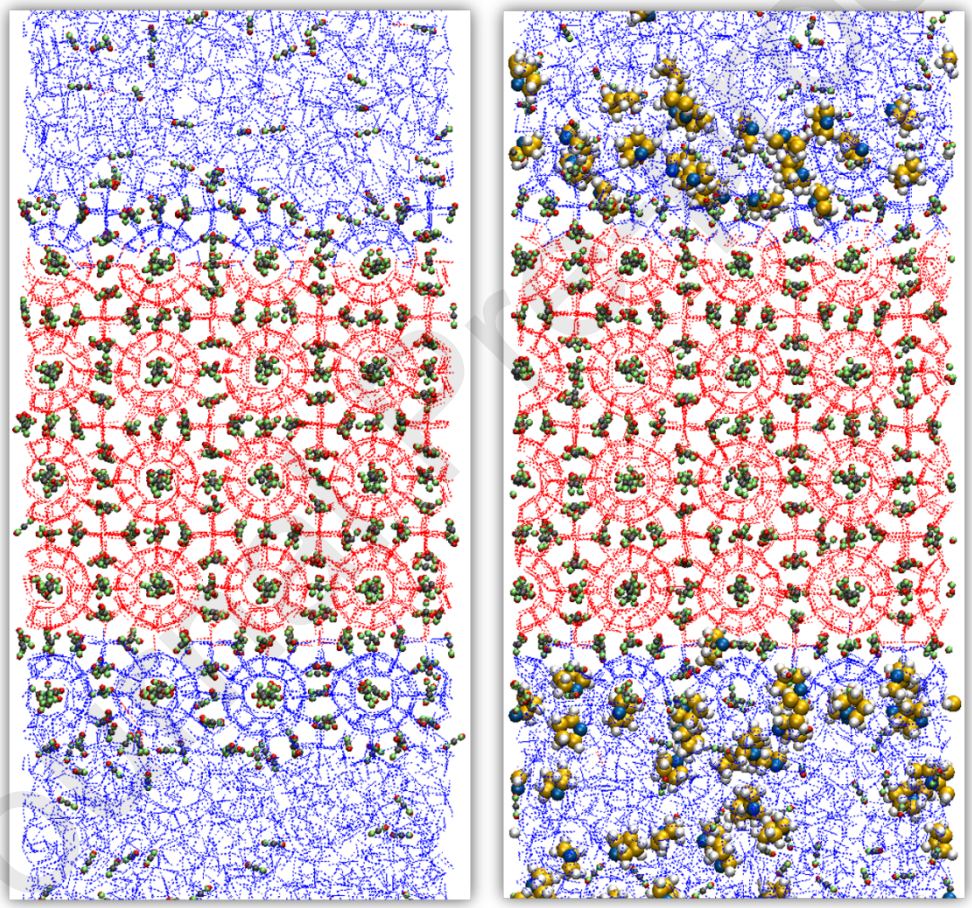

Figure 1. Representative simulation snapshots for the final configurations for systems composed of solid CO_2 hydrate substrate and water, CO_2 without (left) and with (right) THF molecules in the aqueous phase. Blue and red dotted lines symbolise water molecules in the liquid and hydrate phase, respectively. Grey, green and red spheres symbolise CO_2 carbon, dummy, and oxygen atoms, respectively (dummy atoms are required by the implemented model for CO_2). Yellow, white, and blue spheres represent carbon, hydrogen, and oxygen atoms in THF molecules, respectively.

Results and Discussion

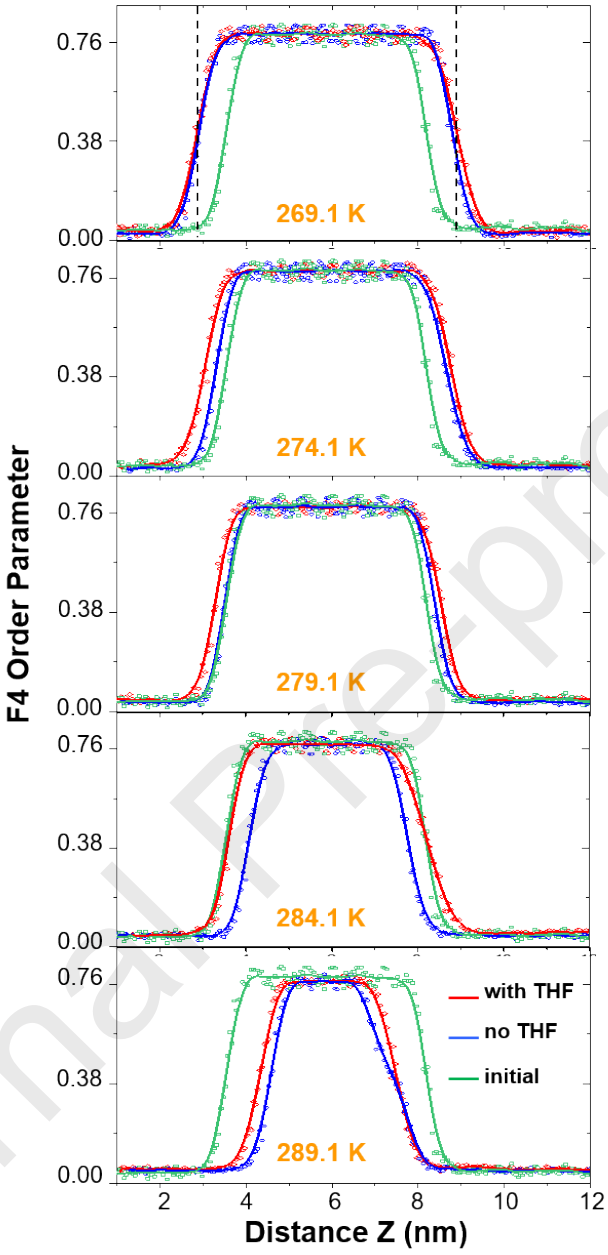

Figure 2. F4 structural order parameter distribution calculated for water molecules along the *Z* direction after 500ns of simulations at the various temperatures. Results were obtained for the systems without (blue) and with (red) THF. The green line indicates the F4 order parameter at the beginning of the simulations. The area between two dotted lines (as illustrated in top panel) represents the region used for estimating the hydrate thickness (details in the text).

CO_2 Gas Hydrate Growth/Dissociation. We quantify the CO_2 gas hydrate growth/dissociation processes at operating conditions by analysing how the F4 structural order parameter for water molecules changes as a function of simulation time, at various temperatures. The F4 order parameter is defined as [62]

$$F4 = \frac{1}{k}\sum_{1}^{k} cos3\emptyset_i \qquad (1)$$

In Eq. (1), $\emptyset$ is the H-O...O-H torsional angle and k is the number of oxygen-oxygen pairs of water molecules found within 0.34 nm of a chosen molecule. The hydrogen atoms used to calculate F4 are the outermost hydrogen atoms in the water dimer. The average values of F4 in a solid hydrate and in liquid water are ~ 0.7 and 0.04, respectively. In our analysis, water molecules are considered part of the hydrate structure when their F4 order parameter is higher than 0.65 [63]. Hence the F4 order parameter can be used to distinguish between the bulk aqueous phase and the hydrate phase within the simulation box [35, 64, 65]. The analysis conducted using the F4 parameter is reliable because no ice was formed in our systems [66].

In **Figure 2**, we present the F4 order parameter distribution along the *Z* direction observed after 500ns of simulations. The results were obtained for systems without (blue) and with (red) THF in the liquid aqueous phase. The simulations were carried out at different temperatures in the range 269.1 to 289.1 K. The results show that the hydrate stability zone (F4 > 0.65) in presence of THF seems to be slightly wider than that observed without THF at 269.1 K and 274.1 K, indicating that THF enhances CO_2 hydrate stability and it is possibly involved in the formation of CO_2–THF binary hydrates at the conditions considered. At higher temperatures (T ≥ 279.1 K), the hydrate is not expected to be stable based on experimental observations [67]. Indeed, the simulation results show that the rate of dissolution of the hydrate in systems without THF increases with temperature more quickly than when THF is present.

To further quantify the impact of THF on the growth/dissociation processes for CO_2 hydrates, we measured the thickness of the hydrate substrate as a function of simulation time for systems with and without THF at various temperatures. The thickness of the hydrate phase is identified by the width of the domain within which the F4 order parameter is larger than 0.65, inclusive of the growing hydrate phase (between the dotted lines illustrated in **Figure 2**, top panel). In **Figure 3**, we report the time evolution of

the hydrate thickness as a function of *T*. The results show that the pure CO_2 hydrates grow at 269.1 and 274.1 K. At 279.1 K, the CO_2 hydrates grow, but they quickly reach a plateau (possibly due to the reduction in the driving force for CO_2 hydrate growth taking place when CO_2 molecules from the bulk and the hydrate-liquid interface are integrated within the growing hydrate). At 284.1 and 289.1 K, the CO_2 hydrates dissociate. When THF is present, the hydrates grow at 269.1 and 274.1 K, but also at 279.1 and at 284.1 K. At 289.1 K, the hydrate dissociates even in the presence of THF. These results are consistent with experimental phase equilibrium data showing that the pure CO_2 hydrates are not stable at temperatures ≥ 279.1 K at 25.5 bar while the CO_2+THF hydrates are stable at temperatures < ~ 288.5 K at ~ 1.42 mol% THF [39, 67]. This suggests that our simulated results describe correctly the thermodynamic properties of pure CO_2 and CO_2+THF hydrates at the selected temperatures and pressures. It should be mentioned that in our simulation set up, as the hydrate grows, CO_2 and THF are consumed from the liquid phase and become part of the hydrate. As a consequence, the driving force that dictates the growth rate decreases as the simulation continues. Salvalaglio and collaborators introduced the Constant Chemical Potential Molecular Dynamics (CμMD) method [68] that could be used to model hydrate growth, and also dissolution, when the driving force is maintained constant. The conclusions presented here would however not change.

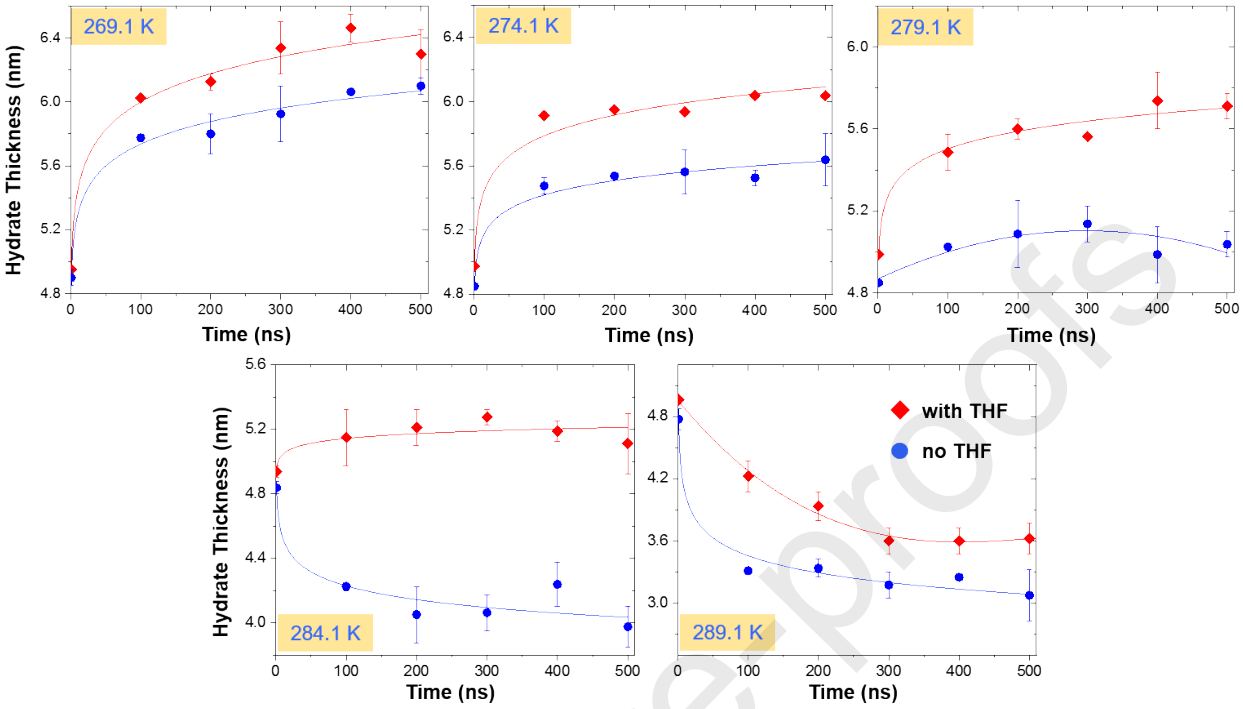

Figure 3. Time evolution of the hydrate thickness. Results were obtained for systems without (blue) and with (red) THF. Different panels are for systems simulated at various temperatures, from 269.1 to 289.1K.

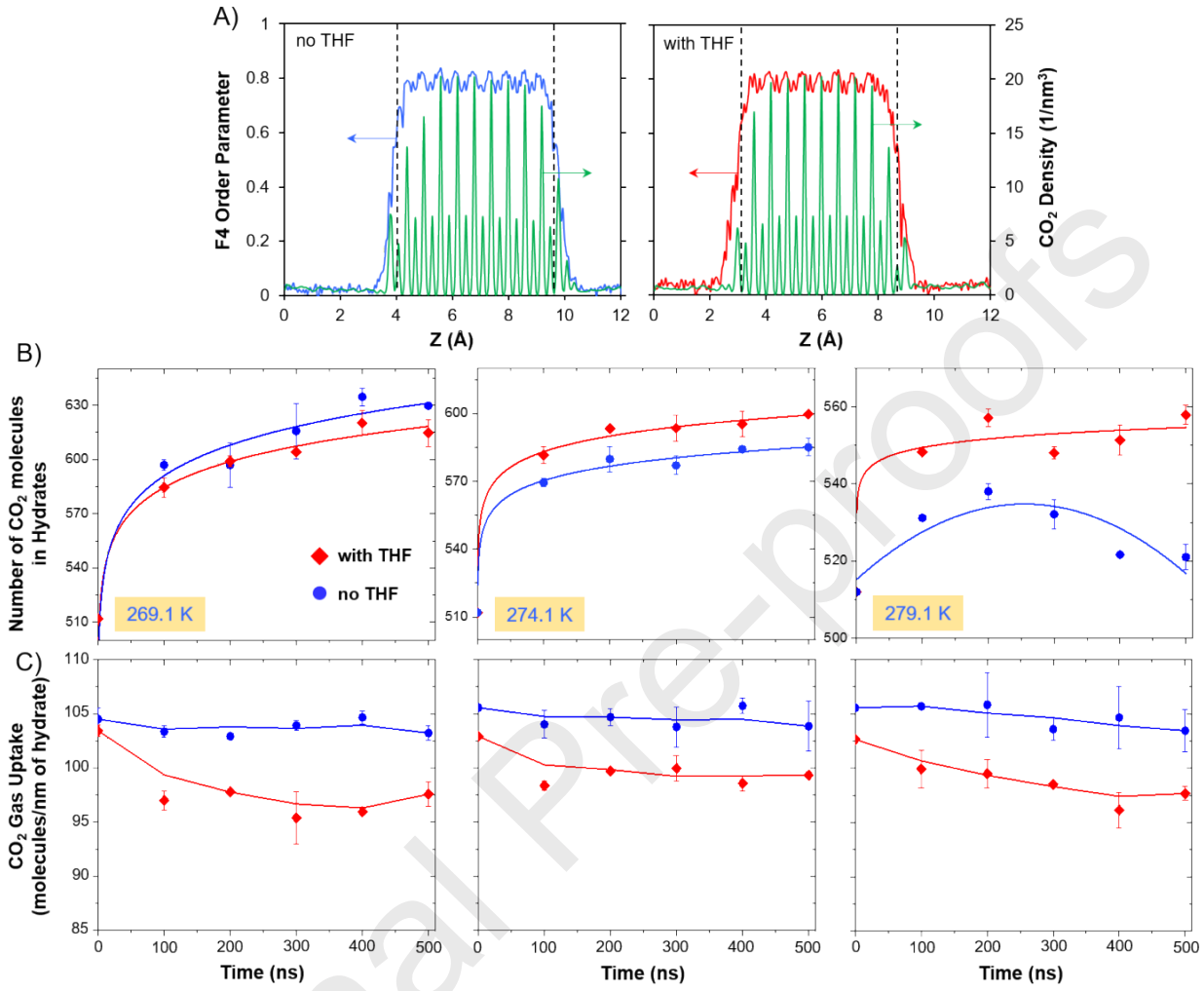

Figure 4. A) F4 order parameter (blue/red) and density profile of CO_2 (green) along the *Z* direction of the simulation box (perpendicular to the hydrate-liquid interface) after 500 ns of simulations conducted at 269.1 K. The area between two dotted lines represents the region used for counting number of CO_2 molecules trapped in the hydrate. B) and C) Number of CO_2 molecules trapped within the hydrate and CO_2 gas uptake in the hydrate phase calculated by dividing the number of CO_2 molecules by the hydrate thickness, respectively, during simulations conducted at 269.1 K (left), 274.1 K (middle), and 279.1 K (right). Systems without (blue) and with (red) THF are compared.

CO_2 Storage Capacity. In **Figure 4**, panel A, we show the density profiles of CO_2 (green) in the *Z* direction for the systems without (left) and with (right) THF after 500ns of simulations conducted at 269.1 K. The results are complemented with data for the F4 order parameter (blue and red, respectively). The CO_2 density profiles show periodic peaks at locations correponding to F4 higher than 0.65, indicating that the

corresponding CO_2 molecules are entrapped in the hydrate phase. To understand how the presence of THF affects the amount of CO_2 captured in the hydrates at different operating conditions, we counted the number of CO_2 molecules in the hydrate phase (identified by the region between the two dotted lines illustrated in **Figure 4A**) as a function of the simualtion time. In **Figure 4B,** the results are reported for systems without (blue) and with (red) THF at 269.1 K (left), 274.1 K (middle), and 279.1 K (right). The results suggest that THF enhances the number of CO_2 molecules trapped in the hydrates at 274.1 and 279.1 K compared to when THF is not used. These results are consistent with the increase of hydrate thickness shown in **Figure 3**. Perhaps surprisingly, at 269.1 K the number of CO_2 molecules in the hydrates for systems without THF is larger than that of systems with THF. This result can be explained considering that at 269.1 K, both pure CO_2 and pure THF hydrates are stable [67, 69]. However, THF-water interactions within the hydrates are stronger than those between CO_2 and water because THF can form hydrogen bonds with water, while CO_2 cannot [70], resulting in more THF occupying the hydrate cages and fewer CO_2 molecules.

Calculating the CO_2 gas uptake in the hydrate phase by dividing the number of CO_2 molecules trapped within the hydrate phase by the hydrate thickness, the results in **Figure 4C** show that the CO_2 gas uptake for systems without THF is larger than that of systems with THF at 269.1, 274.1 and 279.1 K. These results agree well with experimental observations by Veluswamy et al. [32], who found that the CO_2 gas uptake in the hydrate phase is higher than that observed when THF is present, although the experiments were performed at 274.2 and 283.2 K and 30 bar with 5.6% mol THF. It is noteworthy that upon reducing the THF concentration to 1 ÷ 1.5 mol %, which is similar to the one used in our simulations, Lee et al. [39] found that the dissociation boundary was substantially shifted to lower temperatures, e.g. 269.1 K, and higher pressures compared to results obtained with 5.56 mol % THF in the CO_2+THF hydrates. This suggests that our simulation results validate the interpretation of the experimental data proposed by Veluswamy et al. [32], in accordance with which THF in stoichiometric concentration does not improve CO_2 gas uptake. In addition, our simulations suggest that at temperatures at which the pure THF hydrate is not stable, THF shows features similar to those expected from a kinetic promoter as well as from a thermodynamic promoter for CO_2 hydrates.

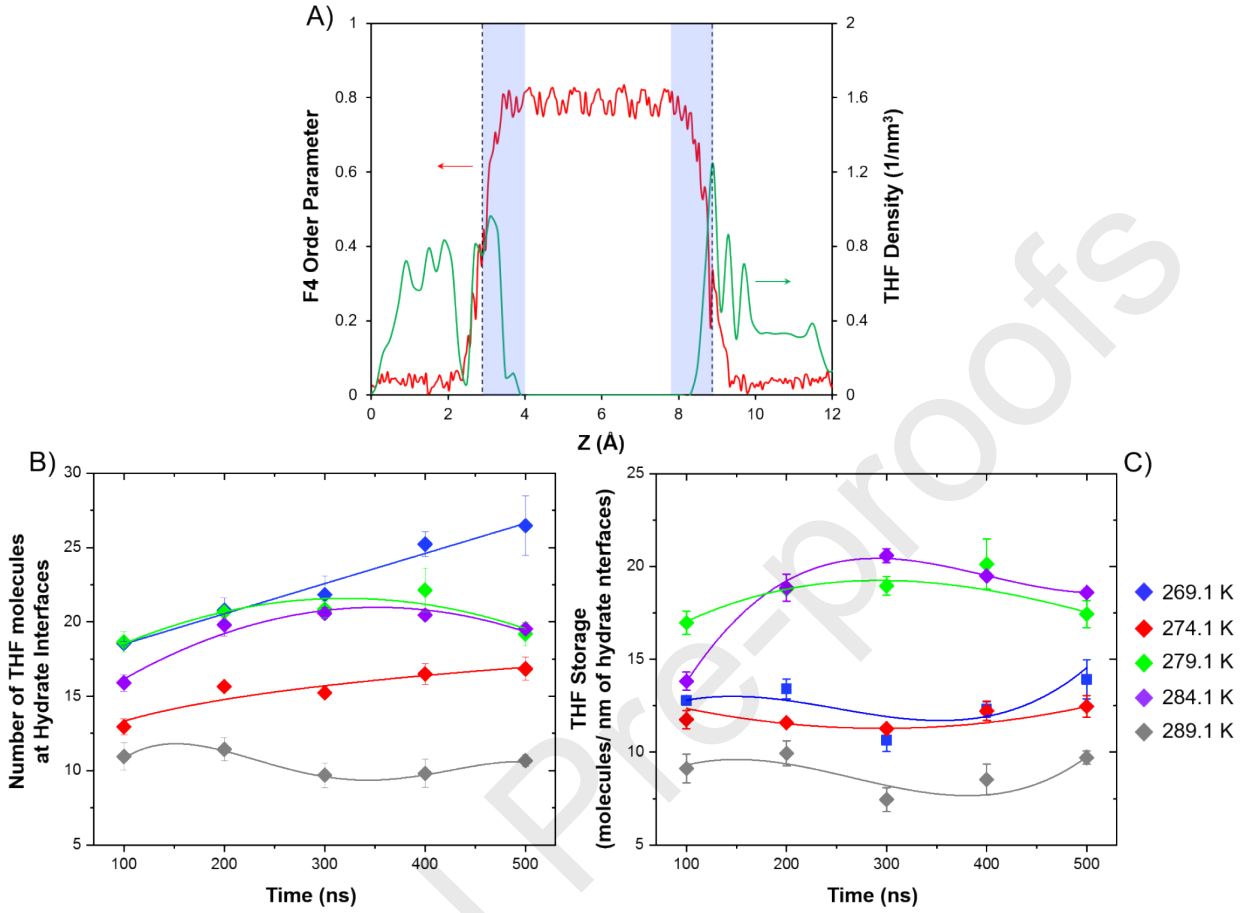

Figure 5. A) F4 order parameter and density profile of THF along the *Z* direction after 500 ns of simulations conducted at 269.1 K. The blue shadow areas represent the hydrate-liquid interfacial regions where THF molecules are trapped. B) Time evolution of the number of THF molecules trapped within the hydrate phase. C) Density of THF computed by dividing the number of THF molecules by the interface thickness as a function of simulation time. Results were obtained at different simulated temperatures.

THF Storage in the Growing Hydrate. To complement the analysis of CO_2 storage capacity, we also report the density profiles of THF along the *Z* direction, together with the distribution of F4 for the system simulated at 269.1 K after 500ns, in **Figure 5A**. The results show that some THF molecules are trapped in the hydrate-liquid interfacial regions (highlighted as blue shadow regions), in which F4 decreases from 0.65 to 0.04. To gain quantitative insights, we calculated the number of THF molecules found in the interfacial regions (blue shadow) and the correspondent density by dividing the number of THF molecules by the

interface thickness as a function of time at different temperatures. The results are shown in **Figure 5B**, left and right panels, respectively.

It is shown that at 269.1 K more THF molecules are stored in the hydrate than at higher temperatures (see **Figure 5B**, left panel). As the simulation progresses, the number of THF molecules confined in the hydrates significantly increases at 269.1 K, while at 274.1 K it increases only slightly; at 279.1 and 284.1 K, it first increases and subsequently decreases, or it remains unchanged with an average 10 THF molecules within the hydrates at 289.1 K. Unexpectedly, many fewer THF molecules are found trapped in the hydrates at 274.1 K than at lower (269.1 K) and higher temperatures (279.1 and 284.1K). The results in Figure 5B, right panel, also show that the THF density in the growing hydrate at 274.1 K is slightly smaller than at lower (269.1 K) while it is much smaller than at higher temperatures (279.1 and 284.1K). These results suggest that 274.1K is perhaps the optimal temperature for THF to act as a promoter for CO_2 hydrates, at which conditions THF seems to function both as a thermodynamic and as a kinetic promoter. It is worth pointing out that the pure THF hydrate starts to dissociate at ~275.8 K at 25.5 bar with ~1.47 mol% THF in the bulk aqueous phase [40], conditions similar to those considered in this study at 274.1 K (25.5 bar and ~1.42% THF). We conclude that at these conditions CO_2 rather than THF preferably occupies the interfacial region near the hydrate phase, as the pure CO_2 hydrate is stable at 274.1K. At higher *T*, the pure CO_2 hydrates dissociate and THF interacts with water more strongly than CO_2 does, yielding to fewer CO_2 molecules trapped in the hydrates. At 289.1 K the CO_2+THF hydrates dissociate (as shown in **Figure 3**), resulting in many fewer THF molecules captured within the hydrate phase than at lower temperatures.

The time evolution of CO_2 and THF molecules trapped within the hydrate phase, as shown in **Figure 4B** and **5B**, suggest that the optimum temperature for CO_2 storage within the growing hydrate when 1.42 mol% THF is present at 25.5 bar is 274.1 K. These results corresponds well with experimental observations from Kim et al., who reported that the CO_2 capture capacity for CO_2+THF hydrate formation is highest at 25 bar and 274.1 K in the presence of 1.5 mol% THF [71].

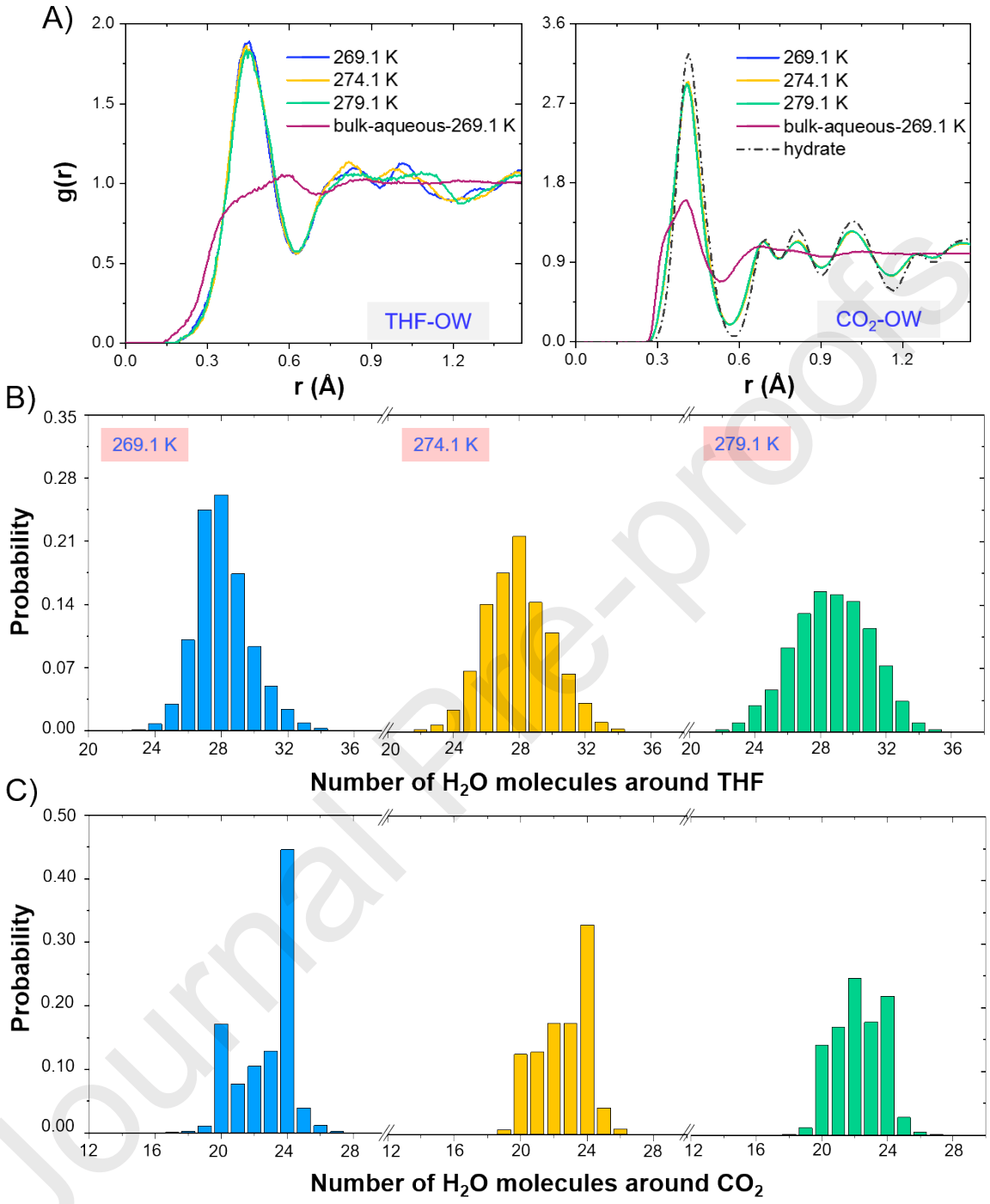

Figure 6. A) Radial distribution functions between the centre of mass of THF molecules and water oxygen atoms (left) and between centre of mass of CO_2 molecules and water oxygen atoms (right) within the hydrate-liquid interfacial regions. B) and C) Probability distribution of the number of water molecules surrounding one THF molecule and one CO_2 molecule within these interfacial regions, respectively. Results were obtained for systems simulated at 269.1 (blue, left), 274.1 (yellow, middle), and 279.1 K (green, right) after 500 ns of simulations. Radial distribution functions between the centre of mass of THF molecules and water oxygen atoms (left) and between centre of mass of CO_2 molecules and water oxygen atoms (right) in the bulk aqueous (red lines) and the bulk hydrate phases (dark grey) at 269.1 K are also shown for comparison.

Hydrate-Liquid Interfacial Structure. Observing CO_2 and THF at the hydrate-liquid interface (i.e., see **Figures 4A** and **5A**) prompts investigations on the probability of forming the commonly expected mixed sII CO_2+THF hydrates in which THF and CO_2 molecules occupy large ($5^{12}6^4$) and small cages (5^{12}), respectively [72]. To quantify this possibility, we computed radial distribution functions (RDF) between the centre of mass of a THF molecule and water oxygen atoms $g_{THF\text{-}OW}(r)$ and between the centre of mass of a CO_2 molecule and water oxygen atoms $g_{CO2\text{-}OW}(r)$. The resultant $g_{THF\text{-}OW}(r)$ and $g_{CO2\text{-}OW}(r)$ are reported in **Figure 6A**, left and right, respectively. The results are shown for the systems simulated at 269.1 K (blue), 274.1 K (yellow), and 279.1 K (green). It is observed that the first peaks in $g_{THF\text{-}OW}(r)$ and $g_{CO2\text{-}OW}(r)$ are located at 4.53 Å and 4.13 Å, respectively, which are within ~0.2 Å of the average cavity radius of large $5^{12}6^4$ (4.73 Å) and small 5^{12} (3.91 Å) cages in the sII hydrate structure [73], respectively. Calculating the $g_{CO2\text{-}OW}(r)$ for CO_2 and water in the bulk hydrate phase (dark grey line), the results show RDF profiles similar to those obtained for the hydrate-liquid interface, which confirms CO_2 being trapping in hydrate cages at the hydrate-liquid interface. Analysis of $g_{THF\text{-}OW}(r)$ and $g_{CO2\text{-}OW}(r)$ within the bulk aqueous phase (red lines) shows significantly less ordered structure of water molecules surrounding THF and CO_2, respectively, compared to the ones found at the hydrate-liquid interface. In addition, we calculated the probability distribution of the number of water molecules surrounding one THF molecule and one CO_2 molecule for the same systems. The results, shown in **Figure 6B** and **6C**, respectively, at 269.1 (blue), 274.1 (yellow), and 279.1 K (green) after 500 ns of simulations, suggest that the probability of observing 28 water molecules around one THF molecule is substantial, which is in good agreement with the presumption that THF would occupy the large $5^{12}6^4$ cages (28 water molecules around THF) in the mixed sII hydrates. Assuming that CO_2 dwells in the small 5^{12} cages of the mixed sII hydrate, 20 water molecules would surround each CO_2 molecule, which is contrary to our results, which show high probability of observing 24 water molecules around each CO_2 molecule (**Figure 6C**). Because our results are consistent with CO_2 molecules being trapped in the large $5^{12}6^2$ cages of sI hydrates, our results are suggesting the possibility of a sub-type of mixed CO_2+THF sII hydrates forming in our system.

To confirm this, we carried out a hydrate cage identification procedure which has been widely used to determine various types of clathrate cages [64, 74-76]. The hydrate cage morphology is characterized based on the hydrogen-bonded networks and the structure of the rings they assemble [77]. The following algorithm was implemented: (1) Determine THF (or CO_2) as guests and the surrounding water molecules within 6.3 Å (or 5.68 Å) (as shown in the RDF in Figure 6A); (2) Two of these water molecules are 'associated' if their O–O distance is shorter than 3.5 Å; (3) Specify all attainable five- and six-membered rings established by 'linked' water molecules [78]; (4) Determine cage type as identified by the number of pentagonal (*P*), the number of hexagonal faces (*H*), and the number of vertices with only two edges.

The probability distribution of finding 5^P6^H cage types surrounding THF and CO_2 within the hydrate-liquid interfacial regions at 269.1 (left), 274.1 (middle), and 279.1 K (right) are shown, respectively, in **Figure 7A** and **7B**. In **Figure 7A** the results show that the probability of observing 5^96^4, $5^{12}6^4$, and 5^76^2 cages surrounding THF is substantial at all temperatures considered. Surprisingly, we find more $5^{12}6^4$ cages at 274.1 than at 269.1 K. Possibly, the THF molecules found in the interfacial regions at 269.1 K could disturb the structure of hydrate cages more strongly than at 274.1 K, leading to the deformation of sII large cage structures. At the higher 279.1 K temperature, the cage structure trapping THF molecules is even more distorted, with evidence of 5^76^2 cages. In **Figure 7B**, it is shown that the probability of observing $5^{12}6^2$ and 5^{12} cages surrounding CO_2 is significant at all temperatures, with a preference for $5^{12}6^2$ cages. This is consistent with the high probability of observing 24 water molecules around CO_2 as discussed in **Figure 6C**. Our results are consistent with experimental results showing low CO_2 occupancy in hydrate 5^{12} cages when THF is present [32], partly leading to low gas uptake for CO_2+THF systems at 269.1 K. In **Figure 7C,** we present a representative simulation snapshot for one $5^{12}6^4$ cage filled with THF and one $5^{12}6^2$ cage filled with CO_2, obtained at 274.1 K after 500 ns of simulations. These results confirm the formation of a sub-type of mixed CO_2+THF sII hydrates where THF and CO_2 occupy $5^{12}6^4$ and $5^{12}6^2$ cages, respectively.

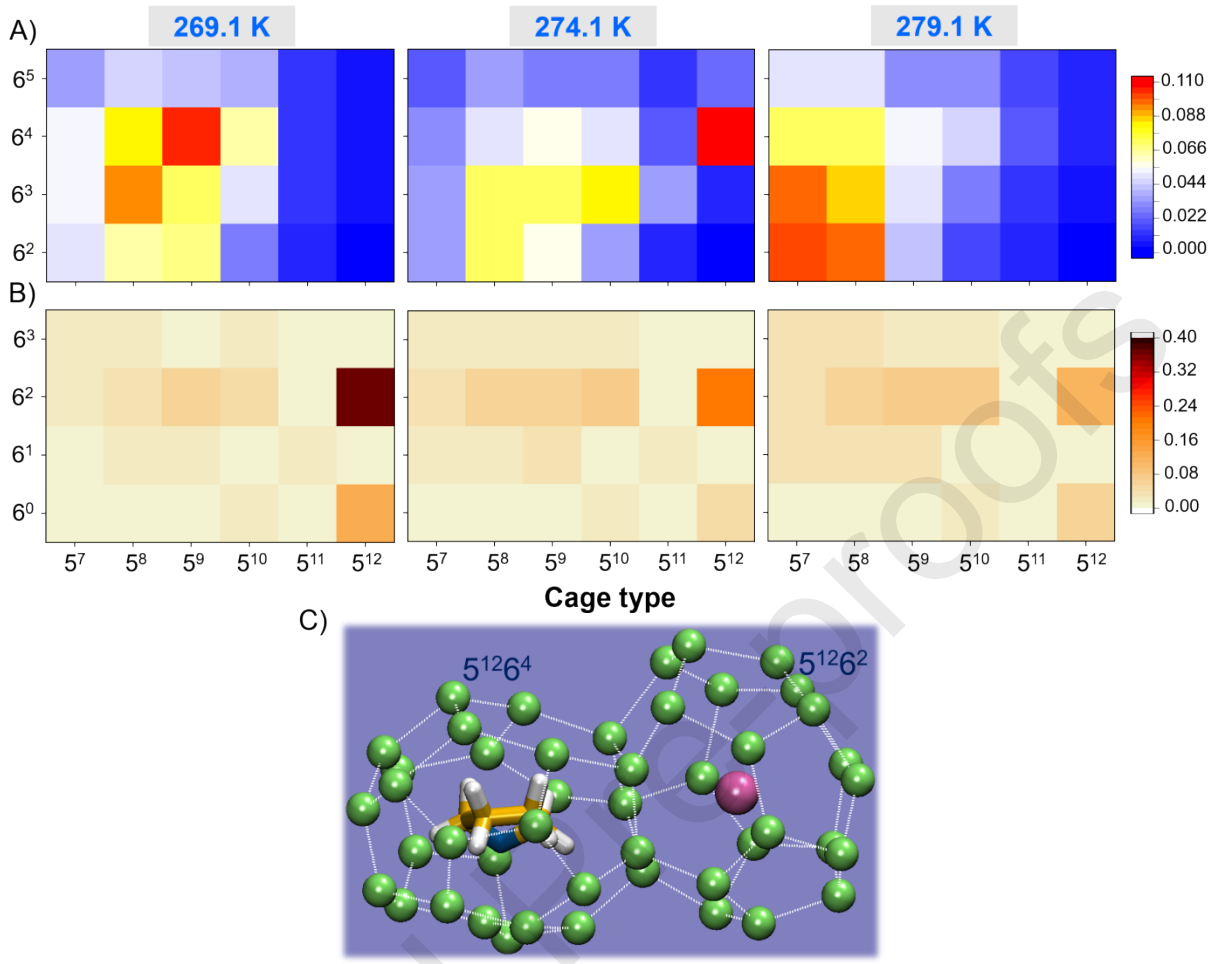

Figure 7. A) and B) Probability distribution of 5^P6^H cage types surrounding THF and CO_2 trapped within hydrate-liquid interfacial regions at 269.1 (left), 274.1 (middle), and 279.1 K (right), respectively. C) Representative simulation snapshot of a $5^{12}6^4$-cage filled with THF and a $5^{12}6^2$-cage holding CO_2. The results were obtained from the system simulated at 274.1 K after 500 ns of simulations.

Dynamic Properties. Analysis of the dynamical properties of CO_2 and THF molecules at the hydrate-liquid interface could help better understand the time evolution of CO_2 and THF molecules captured in the hydrates (e.g., **Figures 4** and **5**). To this end, in **Figure 8** we show the results of the mean square displacement (MSD) for CO_2 and THF molecules within the hydrate-liquid interfacial region. In **Figure 8A**, we report the MSD for CO_2 (left) and THF (right) for system containing THF at different temperatures. The results show that CO_2 travels faster than THF, probably because of its smaller molecular size, as well as its weaker interactions with water [70]. Because the slope of the MSD at long simulation times is

proportional to the diffusion coefficient, our results show that, in general, when the temperature increases, the diffusivity of both CO_2 and THF increases; notwithstanding this, we observe that while the diffusivity of CO_2 increases steadily with temperature, that of THF does not change much at 274.1, 279.1, and 284.1 K. These results are likely due to the higher density of THF present at the hydrate-liquid interface at 279.1 and 284.1 K compared to results obtained at 274.1 K, as discussed in **Figure 5B**. As a result, the resultant THF molecular crowding, more prominent at higher temperatures, contributes to slowing down THF.

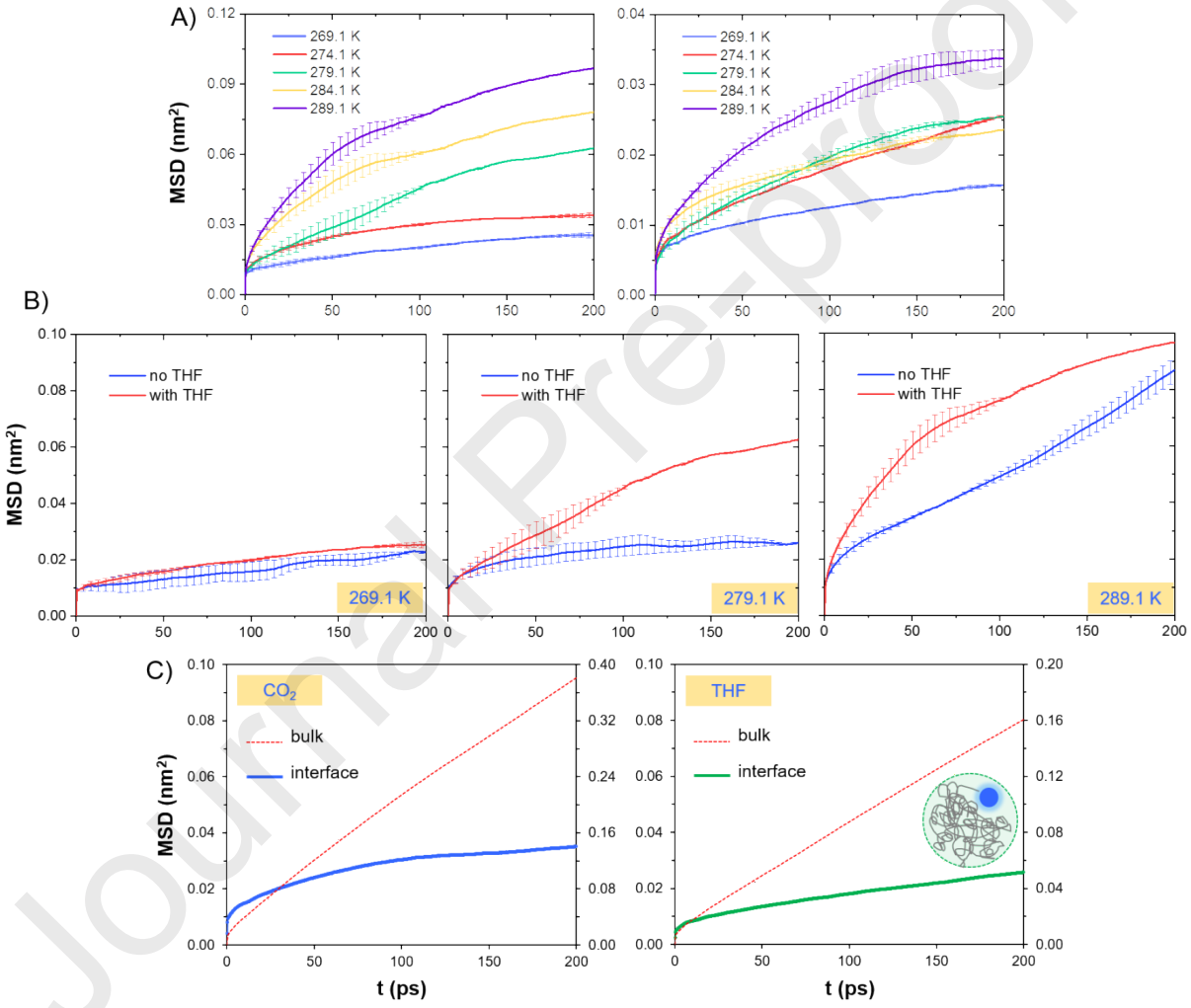

Figure 8. A) Mean square displacement (MSD) for CO_2 (left) and THF (right) molecules in the hydrate-liquid interface. B) Comparison of MSD of CO_2 molecules in the interface for systems without (blue) and with (red) THF. Results are shown for systems simulated at different temperatures. C) Comparison of MSD of CO_2 (left) and THF (right) in the hydrate-liquid interface (blue and right, respectively) and in the bulk aqueous phase (dotted red). Results are from systems with THF at 274.1 K.

In **Figure 8B**, we compare the MSD for CO_2 molecules at the hydrate-liquid interface for systems without THF (blue) and with THF (red). At 269.1 K and 274.1 K (the results at 274.1 K are not shown for brevity), the presence of THF negligibly impacts the dynamical properties of CO_2. At higher temperatures from 279.1 to 289.1 K, however, THF is found to significantly facilitate the diffusivity of CO_2, possibly because the stronger THF-water interactions through hydrogen bonds weaken CO_2-water interactions, opening pathways for CO_2 to travel larger distances. These observations are qualitatively consistent with the experimental results reported by Ripmeester et al., [79] who first showed evidence of enhanced CO_2 cage–to–cage dynamics due to the increased hydrogen bonding probability between THF and water coupled with weakened CO_2–water hydrogen bonding. Ripmeester et al. [79] attributed the facilitated cage-to-cage guest transports to synergistic interactions between guest A–host water–guest B, which expedite guest dynamics in hydrates in the presence of proper guest molecules. It is possible that this enhanced diffusivity at higher temperatures also contributes to the enhancement of CO_2 hydrate formation [39]. It is worth noting that the MSD for both CO_2 and THF at the interface do not grow linearly in time (as shown in **Figure 8C**, blue and green lines, respectively), suggesting anomalous diffusion [80]. Fitting the MSD data with a power function $\langle r^2(t)\rangle \sim t^{\alpha}$, we obtain the value of parameter α to be less than 1, an indication of sub-diffusive behaviour for both CO_2 and THF at the interface. Sub-diffusive diffusion usually occurs in environments classified as 'trapping', 'labyrinthine', and 'viscoelastic' [80], which is consistent with the 'trapping environment' represented by the growing hydrate at the hydrate-liquid interface. For completeness, we also analyse the MSD for CO_2 and THF in the bulk aqueous phase (see **Figure 8C**, dotted red lines, left and right panels, respectively); the results show that these MSDs grow linearly in time, an indication of normal diffusion [80] in the regions where no 'trapping' environments exist.

Conclusions

CO_2 hydrate growth/dissociation processes in presence of THF were studied under a variety of operating conditions using atomistic molecular dynamics simulations. Our simulations indicate that pure CO_2 hydrates are not stable at temperatures ≥ 279.1 K at 25.5 bar while the CO_2+THF hydrates are stable

at temperatures < ~ 288.5 K at ~ 1.42 mol% THF, which is in agreement with experimental phase equilibrium data. The simulated results also show that THF in stoichiometric concentration lessens CO_2 storage capacity at temperatures where the pure THF is stable, due to the low CO_2 occupancy in 5^{12} hydrate cages as well as to the formation of THF–water hydrogen bonds. The analysis of the mobility of different species at interfaces shows that THF significantly enhances the CO_2 diffusion at the hydrate-liquid interface at temperatures ≥ 279.1 K, resulting in the enhancement of CO_2 hydrate formation at these relatively high temperatures. Our study suggests that THF can perform as an effective promoter for CO_2 hydrate formation/growth, with the optimal CO_2 storage in the growing hydrate achieved at conditions at which the pure THF hydrate is not stable while the pure CO_2 is stable. At these conditions, which are identified as 274.1 K at 25.5 bar and ~ 1.42 mol% THF by our simulations, THF yields benefits expected from both thermodynamic and kinetic promoters. The simulation results presented complement available experiments and contribute to a molecular-level understanding of mechanisms responsible for performance of chemical additives in the management and optimization of hydrate-based CO_2 capture and storage.

Conflicts of Interests

There are no conflicts of interests to declare.

Acknowledgments

Financial support was provided by the EPSRC, under grant number EP/T004282/1. Mr. Schlösser was at University College London, on leave from RWTH Aachen University, supported by an Erasmus Plus Fellowship during the completion of the present project. Generous allocations of computing time were provided by ARCHER, the UK National Supercomputing Service (http://www.archer.ac.uk) via our membership of the UK's HEC Materials Chemistry Consortium, which is funded by EPSRC (EP/L000202, EP/R029431), the University College London Research Computing Platforms Support (Grace, Myriad), the Oklahoma Supercomputing Center for Education and Research (OSCER) and the National Energy Research Scientific Computing Center (NERSC) at Lawrence Berkeley National Laboratory. NERSC is

supported by the DOE Office of Science under Contract No. DE-AC02-05CH11231. The authors are grateful to Dr Tai Bui of University College London for fruitful discussions during the preparation of this manuscript.

References

[1] J. Carroll, Natural Gas Hydrates - A Guide for Engineers, Elsevier2003.
[2] Z.M. Aman, C.A. Koh, Interfacial phenomena in gas hydrate systems, Chem Soc Rev 45 (2016) 1678-1690.
[3] A. Striolo, Clathrate hydrates: recent advances on CH4 and CO2 hydrates, and possible new frontiers, Mol Phys (2019).
[4] A. Striolo, A. Phan, M.R. Walsh, Molecular properties of interfaces relevant for clathrate hydrate agglomeration, Curr Opin Chem Eng 25 (2019) 57-66.
[5] P.M. Naullage, A.A. Bertolazzo, V. Molinero, How Do Surfactants Control the Agglomeration of Clathrate Hydrates?, Acs Central Sci 5 (2019) 428-439.
[6] B.J. Anderson, J.W. Tester, G.P. Borghi, B.L. Trout, Properties of inhibitors of methane hydrate formation via molecular dynamics simulations, J Am Chem Soc 127 (2005) 17852-17862.
[7] T. Bui, A. Phan, D. Monteiro, Q. Lan, M. Ceglio, E. Acosta, P. Krishnamurthy, A. StrioloD, Evidence of Structure-Performance Relation for Surfactants Used as Antiagglomerants for Hydrate Management, Langmuir 33 (2017) 2263-2274.
[8] L.E. Zerpa, J.L. Salager, C.A. Koh, E.D. Sloan, A.K. Sum, Surface Chemistry and Gas Hydrates in Flow Assurance, Ind Eng Chem Res 50 (2011) 188-197.
[9] P. Babu, A. Nambiar, T.B. He, I.A. Karimi, J.D. Lee, P. Englezos, P. Linga, A Review of Clathrate Hydrate Based Desalination To Strengthen Energy-Water Nexus, Acs Sustain Chem Eng 6 (2018) 8093-8107.
[10] S.D. Seo, S.Y. Hong, A.K. Sum, K.H. Lee, J.D. Lee, B.R. Lee, Thermodynamic and kinetic analysis of gas hydrates for desalination of saturated salinity water, Chem Eng J 370 (2019) 980-987.
[11] R. Kumar, P. Englezos, I. Moudrakovski, J.A. Ripmeester, Structure and Composition of CO2/H-2 and CO2/H-2/C3H8 Hydrate in Relation to Simultaneous CO2 Capture and H-2 Production, Aiche J 55 (2009) 1584-1594.
[12] N.I. Papadimitriou, I.N. Tsimpanogiannis, I.G. Economou, A.K. Stubos, Monte Carlo simulations of the separation of a binary gas mixture (CH4 + CO2) using hydrates, Phys Chem Chem Phys 20 (2018) 28026-28038.
[13] I. Chatti, A. Delahaye, L. Fournaison, J.P. Petitet, Benefits and drawbacks of clathrate hydrates: a review of their areas of interest, Energ Convers Manage 46 (2005) 1333-1343.
[14] T. Sugahara, J.C. Haag, P.S.R. Prasad, A.A. Warntjes, E.D. Sloan, A.K. Sum, C.A. Koh, Increasing Hydrogen Storage Capacity Using Tetrahydrofuran, J Am Chem Soc 131 (2009) 14616-+.
[15] D.Y. Koh, H. Kang, J. Jeon, Y.H. Ahn, Y. Park, H. Kim, H. Lee, Tuning Cage Dimension in Clathrate Hydrates for Hydrogen Multiple Occupancy, J Phys Chem C 118 (2014) 3324-3330.
[16] M. Khurana, H.P. Veluswamy, N. Daraboina, P. Linga, Thermodynamic and kinetic modelling of mixed CH4-THF hydrate for methane storage application, Chem Eng J 370 (2019) 760-771.
[17] H.P. Veluswamy, A.J.H. Wong, P. Babu, R. Kumar, S. Kulprathipanja, P. Rangsunvigit, P. Linga, Rapid methane hydrate formation to develop a cost effective large scale energy storage system, Chem Eng J 290 (2016) 161-173.
[18] V. Andersson, J.S. Gudmundsson, Flow properties of hydrate-in-water slurries, Gas Hydrates: Challenges for the Future 912 (2000) 322-329.
[19] A. Hassanpouryouzband, E. Joonaki, M.V. Farahani, S. Takeya, C. Ruppel, J.H. Yang, N.J. English, J.M. Schicks, K. Edlmann, H. Mehrabian, Z.M. Aman, B. Tohidi, Gas hydrates in sustainable chemistry, Chem Soc Rev 49 (2020) 5225-5309.
[20] H. Dashti, L.Z. Yew, X. Lou, Recent advances in gas hydrate-based CO2 capture, J Nat Gas Sci Eng 23 (2015) 195-207.

[21] D. Kyung, W. Lee, Structure, stability, and storage capacity of CO2+N2O mixed hydrates for the storage of CO2+N2O mixture gas, Int J Greenh Gas Con 76 (2018) 32-38.
[22] S. Moon, Y.H. Ahn, H. Kim, S. Hong, D.Y. Koh, Y. Park, Secondary gaseous guest-dependent structures of binary neopentyl alcohol hydrates and their tuning behavior for potential application to CO2 capture, Chem Eng J 330 (2017) 890-898.
[23] D. Lee, Y. Lee, J. Lim, Y. Seo, Guest enclathration and structural transition in CO2 + N-2 + methylcyclopentane hydrates and their significance for CO2 capture and sequestration, Chem Eng J 320 (2017) 43-49.
[24] E. Kim, S. Lee, J.D. Lee, Y. Seo, Influences of large molecular alcohols on gas hydrates and their potential role in gas storage and CO2 sequestration, Chem Eng J 267 (2015) 117-123.
[25] A.V. Rayer, P.D. Mobley, M. Soukri, T.R. Gohndrone, J. Tanthana, J. Zhou, M. Lail, Absorption rates of carbon dioxide in amines in hydrophilic and hydrophobic solvents, Chem Eng J 348 (2018) 514-525.
[26] X.W. Zhang, Y.F. Huang, J. Yang, H.X. Gao, Y.Q. Huang, X. Luo, Z.W. Liang, P. Tontiwachwuthikul, Amine-based CO2 capture aided by acid-basic bifunctional catalyst: Advancement of amine regeneration using metal modified MCM-41, Chem Eng J 383 (2020).
[27] E.M. Kutorglo, F. Hassouna, A. Beltzung, D. Kopecky, I. Sedlarova, M. Soos, Nitrogen-rich hierarchically porous polyaniline-based adsorbents for carbon dioxide (CO2) capture, Chem Eng J 360 (2019) 1199-1212.
[28] J. Gibbins, H. Chalmers, Carbon Capture and Storage, Energy Policy 36 (2008) 4317-4322.
[29] Z.W. Ma, P. Zhang, H.S. Bao, S. Deng, Review of fundamental properties of CO2 hydrates and CO2 capture and separation using hydration method, Renew Sust Energ Rev 53 (2016) 1273-1302.
[30] N. Inc., SIMTECHE, L.A.N. Laboratory., Simteche Hydrate CO2 Capture Process 2006.
[31] J.P. Torre, M. Ricaurte, C. Dicharry, D. Broseta, CO2 enclathration in the presence of water-soluble hydrate promoters: Hydrate phase equilibria and kinetic studies in quiescent conditions, Chem Eng Sci 82 (2012) 1-13.
[32] H.P. Veluswamy, K.P. Premasinghe, P. Linga, CO2 Hydrates – Effect of Additives and Operating Conditions on the Morphology and Hydrate Growth, Energy Procedia 105 (2017) 5048-5054.
[33] S.S. Fan, S.F. Li, J.Q. Wang, X.M. Lang, Y.H. Wang, Efficient Capture of CO2 from Simulated Flue Gas by Formation of TBAB or TBAF Semiclathrate Hydrates, Energ Fuel 23 (2009) 4202-4208.
[34] H.P. Veluswamy, S. Kumar, R. Kumar, P. Rangsunvigit, P. Linga, Enhanced clathrate hydrate formation kinetics at near ambient temperatures and moderate pressures: Application to natural gas storage, Fuel 182 (2016) 907-919.
[35] J.Y. Wu, L.J. Chen, Y.P. Chen, S.T. Lin, Molecular dynamics study on the nucleation of methane plus tetrahydrofuran mixed guest hydrate, Phys Chem Chem Phys 18 (2016) 9935-9947.
[36] S.P. Kang, H. Lee, Recovery of CO2 from flue gas using gas hydrate: Thermodynamic verification through phase equilibrium measurements, Environ Sci Technol 34 (2000) 4397-4400.
[37] P. Linga, R. Kumar, J.D. Lee, J. Ripmeester, P. Englezos, A new apparatus to enhance the rate of gas hydrate formation: Application to capture of carbon dioxide, Int J Greenh Gas Con 4 (2010) 630-637.
[38] F. Takeuchi, M. Hiratsuka, R. Ohmura, S. Alavi, A.K. Sum, K. Yasuoka, Water proton configurations in structures I, II, and H clathrate hydrate unit cells, J Chem Phys 138 (2013).
[39] Y.J. Lee, T. Kawamura, Y. Yamamoto, J.H. Yoon, Phase Equilibrium Studies of Tetrahydrofuran (THF) + CH4, THF + CO2, CH4 + CO2, and THF + CO2 + CH4 Hydrates, J Chem Eng Data 57 (2012) 3543-3548.
[40] A. Delahaye, L. Fournaison, S. Marinhas, I. Chatti, J.P. Petitet, D. Dalmazzone, W. Furst, Effect of THF on equilibrium pressure and dissociation enthalpy of CO2 hydrates applied to secondary refrigeration, Ind Eng Chem Res 45 (2006) 391-397.
[41] S.P. Kang, H. Lee, C.S. Lee, W.M. Sung, Hydrate phase equilibria of the guest mixtures containing CO2, N-2 and tetrahydrofuran, Fluid Phase Equilibr 185 (2001) 101-109.
[42] J.L.F. Abascal, E. Sanz, R.G. Fernandez, C. Vega, A potential model for the study of ices and amorphous water: TIP4P/Ice, J Chem Phys 122 (2005).

[43] L. Jensen, K. Thomsen, N. von Solms, S. Wierzchowski, M.R. Walsh, C.A. Koh, E.D. Sloan, D.T. Wu, A.K. Sum, Calculation of Liquid Water-Hydrate-Methane Vapor Phase Equilibria from Molecular Simulations, J Phys Chem B 114 (2010) 5775-5782.
[44] M.R. Walsh, C.A. Koh, E.D. Sloan, A.K. Sum, D.T. Wu, Microsecond Simulations of Spontaneous Methane Hydrate Nucleation and Growth, Science 326 (2009) 1095-1098.
[45] J.G. Harris, K.H. Yung, Carbon Dioxide's Liquid-Vapor Coexistence Curve And Critical Properties as Predicted by a Simple Molecular Model, J Phys Chem-Us 99 (1995) 12021-12024.
[46] Y.T. Tung, L.J. Chen, Y.P. Chen, S.T. Lin, Growth of Structure I Carbon Dioxide Hydrate from Molecular Dynamics Simulations, J Phys Chem C 115 (2011) 7504-7515.
[47] J.M. Miguez, M.M. Conde, J.P. Torre, F.J. Blas, M.M. Pineiro, C. Vega, Molecular dynamics simulation of CO2 hydrates: Prediction of three phase coexistence line, J Chem Phys 142 (2015).
[48] P. Procacci, PrimaDORAC: A Free Web Interface for the Assignment of Partial Charges, Chemical Topology, and Bonded Parameters in Organic or Drug Molecules, J Chem Inf Model 57 (2017) 1240-1245.
[49] J.W. Eastwood, R.W. Hockney, D.N. Lawrence, P3m3dp - the 3-Dimensional Periodic Particle-Particle-Particle-Mesh Program, Comput Phys Commun 19 (1980) 215-261.
[50] M.P. Allen, D.J. Tildesley, Computer Simulation of Liquids, Oxford University Press, Oxford, UK, 2004.
[51] B. Hess, C. Kutzner, D. van der Spoel, E. Lindahl, GROMACS 4: Algorithms for highly efficient, load-balanced, and scalable molecular simulation, J Chem Theory Comput 4 (2008) 435-447.
[52] D. Van der Spoel, E. Lindahl, B. Hess, G. Groenhof, A.E. Mark, H.J.C. Berendsen, GROMACS: Fast, flexible, and free, J Comput Chem 26 (2005) 1701-1718.
[53] S. Nose, A Molecular-Dynamics Method for Simulations in the Canonical Ensemble, Mol Phys 52 (1984) 255-268.
[54] W.G. Hoover, Canonical Dynamics - Equilibrium Phase-Space Distributions, Phys Rev A 31 (1985) 1695-1697.
[55] Y. Zhang, E.J. Maginn, A comparison of methods for melting point calculation using molecular dynamics simulations, J Chem Phys 136 (2012).
[56] M.M. Conde, C. Vega, Determining the three-phase coexistence line in methane hydrates using computer simulations, J Chem Phys 133 (2010).
[57] T. Yagasaki, M. Matsumoto, H. Tanaka, Formation of Clathrate Hydrates of Water-Soluble Guest Molecules, J Phys Chem C 120 (2016) 21512-21521.
[58] T. Yagasaki, M. Matsumoto, H. Tanaka, Mechanism of Slow Crystal Growth of Tetrahydrofuran Clathrate Hydrate, J Phys Chem C 120 (2016) 3305-3313.
[59] M. Parrinello, A. Rahman, Polymorphic Transitions in Single-Crystals - a New Molecular-Dynamics Method, J Appl Phys 52 (1981) 7182-7190.
[60] R.W. Hockney, S.P. Goel, J.W. Eastwood, Quiet High-Resolution Computer Models of a Plasma, J Comput Phys 14 (1974) 148-158.
[61] S. Sarupria, P.G. Debenedetti, Molecular Dynamics Study of Carbon Dioxide Hydrate Dissociation, J Phys Chem A 115 (2011) 6102-6111.
[62] P.M. Rodger, T.R. Forester, W. Smith, Simulations of the methane hydrate methane gas interface near hydrate forming conditions, Fluid Phase Equilibr 116 (1996) 326-332.
[63] T. Bui, F. Sicard, D. Monteiro, Q. Lan, M. Ceglio, C. Burress, A. Striolo, Antiagglomerants Affect Gas Hydrate Growth, J Phys Chem Lett 9 (2018) 3491-3496.
[64] K.W. Hall, S. Carpendale, P.G. Kusalik, Evidence from mixed hydrate nucleation for a funnel model of crystallization, P Natl Acad Sci USA 113 (2016) 12041-12046.
[65] S. Liang, P.G. Kusalik, Exploring nucleation of H2S hydrates, Chem Sci 2 (2011) 1286-1292.
[66] A.H. Nguyen, V. Molinero, Identification of Clathrate Hydrates, Hexagonal Ice, Cubic Ice, and Liquid Water in Simulations: the CHILL plus Algorithm, J Phys Chem B 119 (2015) 9369-9376.

[67] S. Adisasmito, R.J. Frank, E.D. Sloan, Hydrates of Carbon-Dioxide and Methane Mixtures, J Chem Eng Data 36 (1991) 68-71.
[68] C. Perego, M. Salvalaglio, M. Parrinello, Molecular dynamics simulations of solutions at constant chemical potential, J Chem Phys 142 (2015).
[69] T. Makino, T. Sugahara, K. Ohgaki, Stability boundaries of tetrahydrofuran plus water system, J Chem Eng Data 50 (2005) 2058-2060.
[70] M.J. Shultz, T.H. Vu, Hydrogen Bonding between Water and Tetrahydrofuran Relevant to Clathrate Formation, J Phys Chem B 119 (2015) 9167-9172.
[71] S. Kim, S.H. Lee, Y.T. Kang, Characteristics of CO2 hydrate formation/dissociation in H2O + THF aqueous solution and estimation of CO2 emission reduction by district cooling application, Energy 120 (2017) 362-373.
[72] Q. Sun, Y.T. Kang, Review on CO2 hydrate formation/dissociation and its cold energy application, Renew Sust Energ Rev 62 (2016) 478-494.
[73] E. Dendy Sloan, Fundamental principles and applications of natural gas hydrates, Nature 426 (2003) 353-359.
[74] G.J. Guo, Y.G. Zhang, C.J. Liu, K.H. Li, Using the face-saturated incomplete cage analysis to quantify the cage compositions and cage linking structures of amorphous phase hydrates, Phys Chem Chem Phys 13 (2011) 12048-12057.
[75] K.W. Hall, Z.C. Zhang, P.G. Kusalik, Unraveling Mixed Hydrate Formation: Microscopic Insights into Early Stage Behavior, J Phys Chem B 120 (2016) 13218-13223.
[76] S.X. Li, R.J. Lv, Z.S. Yan, F. Huang, X.R. Zhang, G.J. Chen, T.T. Yue, Design of Alanine-Rich Short Peptides as a Green Alternative of Gas Hydrate Inhibitors: Dual Methyl Group Docking for Efficient Adsorption on the Surface of Gas Hydrates, Acs Sustain Chem Eng 8 (2020) 4256-4266.
[77] L.C. Jacobson, W. Hujo, V. Molinero, Thermodynamic Stability and Growth of Guest-Free Clathrate Hydrates: A Low-Density Crystal Phase of Water, J Phys Chem B 113 (2009) 10298-10307.
[78] M. Matsumoto, A. Baba, I. Ohmine, Topological building blocks of hydrogen bond network in water, J Chem Phys 127 (2007).
[79] I.L. Moudrakovski, K.A. Udachin, S. Alavi, C.I. Ratcliffe, J.A. Ripmeester, Facilitating guest transport in clathrate hydrates by tuning guest-host interactions, J Chem Phys 142 (2015).
[80] Y. Meroz, I.M. Sokolov, A toolbox for determining subdiffusive mechanisms, Phys Rep 573 (2015) 1-29.

Highlights

- THF act both as thermodynamic and kinetic promoter for CO_2 hydrates.
- At the optimal conditions, THF facilitates CO_2 diffusion and hydrate growth.
- Molecular simulations can be used to optimise CCS processes.

Graphical Abstract

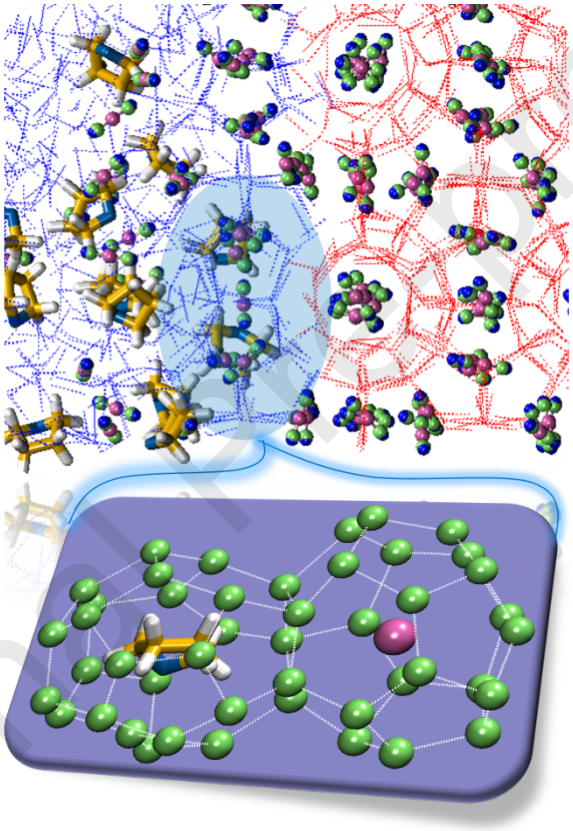

Highlights

- THF act both as thermodynamic and kinetic promoter for CO_2 hydrates.
- At the optimal conditions, THF facilitates CO_2 diffusion and hydrate growth.
- Molecular simulations can be used to optimise CCS processes.

Conflicts of Interests

The Authors declare no conflicts of interest.